Werk

Jahr: 1981
Kollektion: fid.geo
Signatur: 8 Z NAT 2148:49
Digitalisiert: Niedersächsische Staats- und Universitätsbibliothek Göttingen
Werk Id: PPN1015067948_0049
PURL: http://resolver.sub.uni-goettingen.de/purl?PPN1015067948_0049

LOG Id: LOG_0036
LOG Titel: Observations of field-aligned current sheets above discrete auroral arcs
LOG Typ: article

Übergeordnetes Werk

Werk Id: PPN1015067948
PURL: http://resolver.sub.uni-goettingen.de/purl?PPN1015067948
OPAC: http://opac.sub.uni-goettingen.de/DB=1/PPN?PPN=1015067948

Contact

Niedersächsische Staats- und Universitätsbibliothek Göttingen
Georg-August-Universität Göttingen
Platz der Göttinger Sieben 1
37073 Göttingen
Germany
Email: gdz@sub.uni-goettingen.de

J Geophys (1981) 49:128–137

Journal of Geophysics

Observations of Field-Aligned Current Sheets Above Discrete Auroral Arcs

K. Wilhelm[1], N. Klöcker[2], B. Theile[2], W. Ott[3], K. Spenner[3], R. Grabowski[3], H. Wolf[3], W. Stüdemann[1], G. Dehmel[4], H.M. Fischer[5], G.L. Schmidtke[5], W. Baumjohann[6], W. Riedler[7], and A. Urban[8]

[1] Max-Planck-Institut für Aeronomie, D-3411 Katlenburg-Lindau 3, Federal Republic of Germany
[2] Institut für Geophysik und Meteorologie der Technischen Universität Braunschweig, D-3300 Braunschweig, Federal Republic of Germany
[3] Fraunhofer Institut für physikalische Meßtechnik, D-7800 Freiburg, Federal Republic of Germany
[4] Institut für Nachrichtentechnik der Technischen Universität Braunschweig, D-3300 Braunschweig, Federal Republic of Germany
[5] Institut für Reine und Angewandte Kernphysik der Universität Kiel, D-2300 Kiel, Federal Republic of Germany
[6] Institut für Geophysik der Universität Münster, D-4400 Münster/Westfalen, Federal Republic of Germany
[7] Institut für Nachrichtentechnik und Wellenausbreitung der Technischen Universität Graz, A-8010 Graz, Austria
[8] Institut für Weltraumforschung der Österreichischen Akademie der Wissenschaften, A-8010 Graz, Austria

Abstract. A high-altitude sounding rocket payload was launched into an auroral break-up event from the Andøya Rocket Range on 13 October 1977. The comprehensive experiment complement of the payload allowed particle and field observations over wide energy and frequency ranges. In addition, good coverage of the event was provided by ground-based instrumentation. The payload encountered at least two well-developed current sheets at the northern boundary of the auroral activity and westward electrojet region. In the upward-directed current regimes, with widths of approximately 10 km and current densities of up to 40 $\mu A\ m^{-2}$, the charge carriers were, predominantly, precipitating energetic electrons embedded in a low-density, high-temperature magnetospheric plasma. The downward-directed currents, on the other hand, were accompanied by a high-density, low-temperature plasma. Signatures of the current sheets could also be identified in the perpendicular electric field as abrupt intensity and direction variations as well as in spectral modifications of high-energy electron and proton fluxes.

Key words: Auroral arcs – Field-aligned current sheets

Introduction

The understanding of the complex physical processes leading to the generation of auroral displays was significantly advanced when it became clear that low-altitude acceleration of electrons played an important rôle in the energy and mass transfer above discrete auroral arcs (Evans 1974; Mende and Shelley 1976; Kaufmann et al. 1976; Mizera and Fennell 1977; Raitt and Sojka 1977, Bryant et al. 1977; Croley et al. 1978; Cattell et al. 1979, Wilhelm 1979). Both theoretical considerations and experimental evidence supported the conclusion that magnetically aligned electric fields were responsible for the acceleration and subsequent precipitation of magnetospheric electrons into the ionosphere (Swift 1978, 1979; Kan and Akasofu 1979). However, the subject is still very controversial, and evidence that a straightforward electrostatic acceleration of charged particles is inconsistent with many observations has recently been summarized by Whalen and Daly (1979).

The downward flow of energetic auroral electrons forms part of a large-scale system of Birkeland currents connecting the outer magnetosphere with the ionosphere (Anderson and Vondrak 1975). In the same region, upward-directed ion beams have been observed adding to the electric current density (Sharp et al. 1979). The identification of the charge carriers of the currents into the ionosphere has not been accomplished unambigiously, although the current flow has been clearly detected by magnetometer observations from satellites and sounding rockets (Zmuda et al. 1970; Theile and Praetorius 1973; Armstrong et al. 1975). Theile and Praetorius (1973) demonstrated that the field-aligned currents occurred above auroral arcs. In a recent paper, Cattell et al. (1979) discussed the consequences of different particle populations in regions with upward- or downward-directed currents. It was assumed that the plasma carrying downward currents would be populated by cold, high-density, ionospheric electrons and that upward current regions could be characterized by relatively low-density, hot, magnetospheric electron populations.

In this paper, we present a comprehensive set of measurements made by an experiment complement aboard a sounding rocket during an auroral break-up event. The observations demonstrate the above assumption directly and, moreover, relate the transitions between the different plasma regions to electrostatic field transitions. The high time-resolution available combined with the relatively low horizontal velocity of the payload provided a spatial resolution of less than 30 m, assuming the current structure to be at rest with respect to the earth's surface.

Instrumentation

The payload under discussion here was part of a sounding rocket programme, named "Substorm Phenomena" Identical experiment complements in four payloads were selected to provide a set of plasma, particle and field observations during various phases of magnetospheric substorm events. Details of the experiments are compiled in Table 1 which also indicates the various institutions responsible for the particular instrument developments.

The payloads were launched by Skylark 12 motors from the Andøya Rocket Range, Norway, and flight 3A, which we consider here, reached a peak altitude of 536.4 km. All experiments and

0340-062X/81/0049/0128/$02.00

Table 1. List of experiments flown aboard the payloads "Substorm phenomena"

Experiment	Technique	Measurements	Institution
Electric field experiment			
DCTF 3	2 boom-mounted double probe sensors	DC electric field resolution 0.1 1 mV/m	IPM, Freiburg
ACTN 1		AC electric field 50 Hz–20 kHz	ESTEC, Noordwijk
Förster' magnetometer TS 1	3-component fluxgate magnetometer	DC magnetic field 0–500 Hz, resolution 1 nT	TU, Braunschweig
AC magnetometer TS 2	1-component search coil	Magnetic component of wave fields 50 Hz–5 kHz	TU, Braunschweig
Plasma experiment TF 4	Retarding potential analyser	Electron temperature, ion density ion wind, vehicle potential electron flux 0–30 eV	IPM, Freiburg
Particle spectrometer Electrons TL 7 Protons TZ 1	Hemispherical electrostatic analyser and open electron multipliers	Electron and proton fluxes $0.1(1) \leqq E_e(E_p) \leqq 25(40)$ keV	MPAE, Lindau INW, Graz
Particle spectrometer TL 6	Magnetic particle analyser and solid-state detectors	Electron and proton fluxes $20(40) \leqq E_e(E_p) \leqq 200(300)$ keV	MPAE, Lindau
Particle spectrometer TK 1	Solid-state detector telescope	Proton fluxes $0.07 \leqq E_p \leqq 2$ MeV	IFKKI, Kiel

other subsystems worked perfectly thus providing a wealth of data, some of which will be discussed in this paper. The payload was controlled in attitude so as to point $20° \pm 10°$ off the negative geomagnetic field direction and had a spin period of 350 ms.

Geophysical Conditions During Launch

The payload flew on 13 October 1977 during a magnetospheric substorm starting at 20:22 UT and lasting until 23:30 UT Two auroral break-ups occurred during this substorm. The variations of the magnetic field components recorded at Andenes as displayed in Fig. 1 provide an overview of the situation which occurred during a period of moderate planetary geomagnetic disturbance levels with Kp=3− Except during the first 40 min of the substorm, both the positive and negative variations of the Z and Y components were less than 100 nT, while X reached a minimum of −400 nT Of particular interest is the time interval 20:48–20:55 UT, characterized by strong negative Z variation. The corresponding auroral forms showed a violent disruption of the east-west oriented band with, at times, nearly north-south directed curtains.

While the X-component attained large negative values, the auroral activity subsequently concentrated in a faint homogeneous arc with sharp northern boundary which moved slowly southwards. Based on the decreasing X-component, an intensification of the arc and a slight enhancement of the geomagnetic micropulsation activity at 21:22 UT, the rocket was fired at 21:26 UT Shortly after launch, the arc brightened to an intensity of more than 50 kR in the 557.7 nm oxygen line. The payload crossed the arc two minutes later and reached the northern boundary of the auroral activity at about 21.30 UT The measurements of the Andenes scanning photometer are displayed in a time-distance coordinate system in Fig. 2 for the 557.7 nm auroral line. It can be seen that at 21:31 UT an auroral break-up occurred with rapid expansion of the aurora to the north. Further information on the geophysical conditions during the flight has been compiled elsewhere (Wilhelm 1980). Without discussion it should be pointed out that a fading of the auroral brightness occurred before

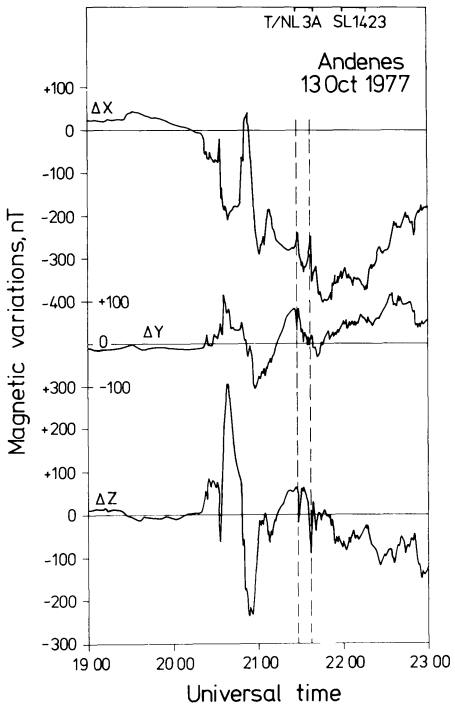

Fig. 1. Variations of the geomagnetic field at Andenes on 13 October 1977. The variations of the north, east and vertical components are denoted by ΔX, ΔY, and ΔZ, respectively. The flight times of the two sounding rocket payloads T/NL 3A and SL 1423 (the latter not discussed in this paper) have been indicated. Note the two impulsive changes of ΔX at 21:27 UT and 21 35 UT The pulse at 21:27 UT coincided with an auroral break-up

the break-up similar to the observations by Pellinen and Heikkila (1978). The sequence of events has been documented by all-sky photographs from Andenes shown in Fig. 3. The trajectory of the payload has been projected downwards along the magnetic field lines to an altitude of 120 km and has been overlaid on both the photometer and the all-sky camera data in order to

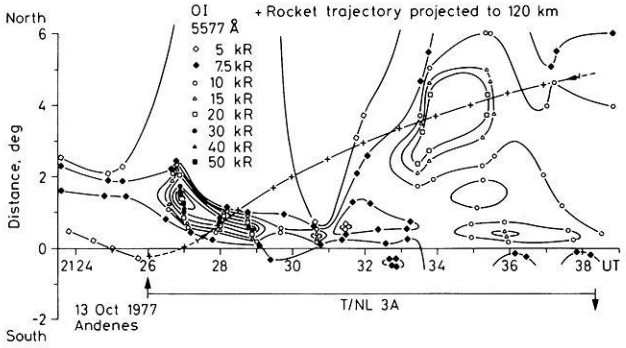

Fig. 2. Isophotes of the green oxygen line at 557.7 nm presented in a spatial-temporal co-ordinate system and derived from scanning photometer observations. The distance is measured from the launch site on an azimuth of 340° corresponding to the launch direction of the rocket. The rocket trajectory projected down along the local magnetic field direction to a height of 120 km is also shown

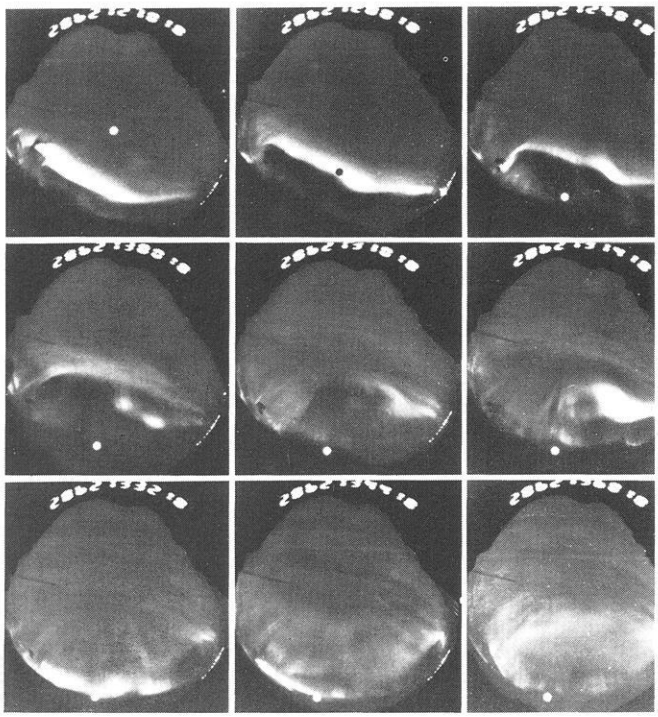

Fig. 3. All-sky camera photographs during the flight of payload T/NL 3A. The frames (from left to right) were taken at approximately 1 min intervals at 21:27:01, 28:01, 29:01, 30:01, 31:01, 31:41, 33:21, 34:41, and 36:01, respectively. The exposure time was 16 s. North is at the bottom of the frames and east to the right. The instantaneous position of the payload was projected down to an altitude of 120 km and marked by *dots* in the frames of this figure

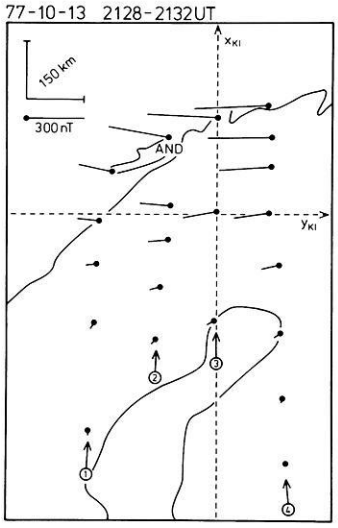

Fig. 4. Averaged equivalent current vectors on the earth's surface showing the direction of the current and the magnitude of the disturbance field. The current vectors have their origin at the station where the corresponding magnetic disturbances were observed (the station denoted by AND is located at the Andøya rocket range). The numbers in circles denote the different profiles. The co-ordinate system is explained in the text

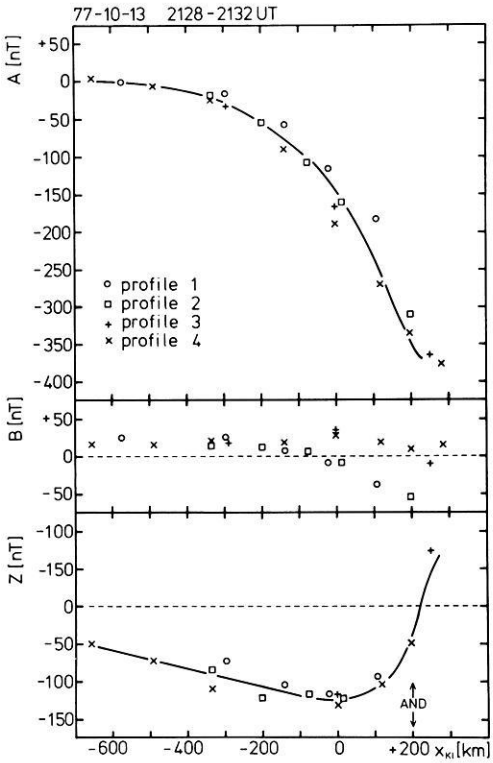

Fig. 5. Latitudinal distribution of 4 min averaged magnetic components observed on four different profiles (see Fig. 4). The *solid lines* denote *A* and *Z* components averaged over the profiles. Also indicated is the location of the Andøya rocket range (*AND*)

establish the spatial relationship of the auroral forms with respect to the payload. The riometer recording at Andenes on 27.6 MHz showed a relatively smooth absorption event of approximately 0.9 dB over the flight.

The observations and subsequent discussion pertain to small-scale phenomena observed by the instrumentation of the payload. The prevailing large scale electrojet configuration was observed by the Scandinavian Magnetometer Array (Küppers et al. 1979). Analysis has been carried out for the interval between 2128 and 2132 UT. Since the gross spatial configuration of the magnetic field did not change and an increase of only 10% in amplitude was observed during this interval, it should suffice to consider values averaged over 4 min in the following discussion.

In Fig. 4 the averaged equivalent currents, in terms of their magnetic field amplitude at the earth's surface, are displayed, whereas Fig. 5 shows the amplitudes, averaged in time, of the north, east and vertical magnetic components along the x_{KI} axis.

The coordinate system used in Fig. 4 is a Cartesian system obtained by a projection of the globe onto a tangential plane centred at Kiruna, Sweden. The y_{KI} axis of the system has been chosen as the tangent to the projection of the ϕ_c (KIR)=64.8° line with ϕ_c being the revised corrected geomagnetic latitude as given by Gustafsson (1970). The x_{KI} axis is perpendicular to the y_{KI} axis and is directed approximately 12° west of geographic north at Kiruna.

Both figures show that a westward electrojet was centred near x_{KI}=200–250 km decreasing slightly in strength in the westward direction. The southward-directed equivalent currents in sub-auroral latitudes and the distribution of the B components (parallel to y_{KI}) along the x_{KI} axis seem to indicate a divergence of the westward electrojet. Whether this divergence was balanced by upward-flowing field-aligned currents (Hughes and Rostoker 1977, 1979; Baumjohann 1979) remains to be determined.

As can be seen in Fig. 17, the large-scale ionospheric electric field is directed southwards. The westward electrojet could therefore be attributed to an ionospheric Hall current. In order to calculate the height-integrated ionospheric Hall current density we have applied the method of field separation and subsequent upward continuation (Mersmann et al. 1979; Baumjohann et al. 1979) to the averaged latitudinal profiles of the A and Z components displayed in Fig. 5. As no magnetic field data were available north of the Norwegian coast the assumption was made that the A and Z components were symmetric and anti-symmetric with respect to x_{KI}=200–250 km.

The resulting x_{KI} profile of the height-integrated westward Hall current density at 100 km height is shown in Fig. 6. It can be seen that the westward electrojet has its maximum height-integrated current density of about 8×10^5 μAm^{-1} slightly north of Andøya and close to the region of maximum auroral luminosity. The main part of the current was confined to a region of $\pm$300 km around this maximum. The northern boundary of the current flow was close to the boundary of the auroral activity as indicated by the rocket results, which supports our earlier assumption of a symmetric current flow.

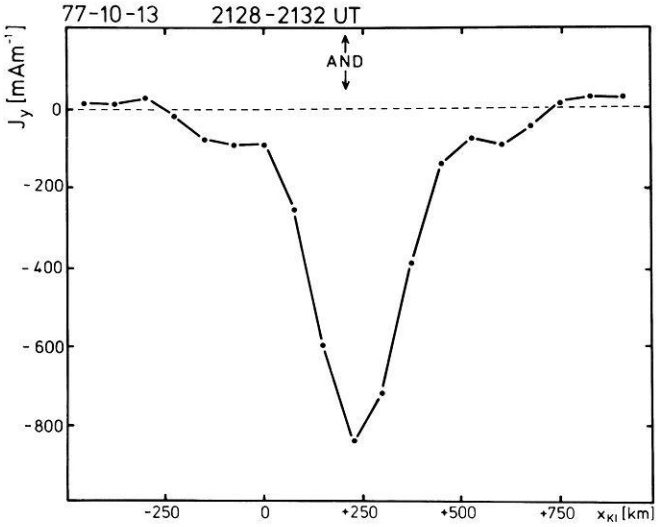

Fig. 6. Latitudinal distribution of the height-integrated Hall current density. Also indicated is the location of the Andøya rocket range (*AND*). The current density north of Andenes was calculated assuming symmetry

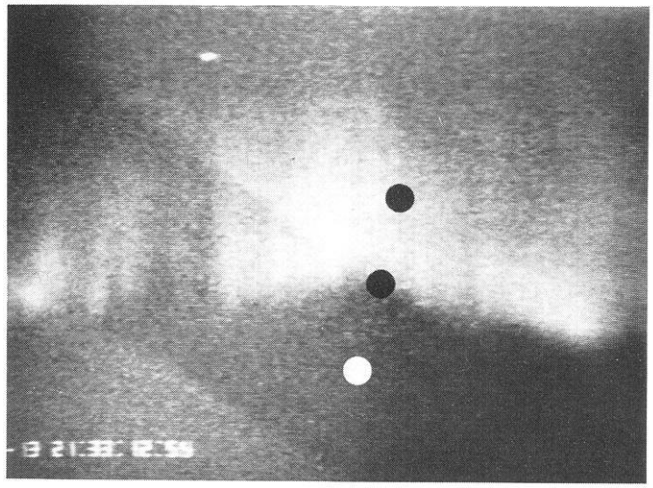

Fig. 7. Active auroral from overflown by the payload shortly before this TV observation was made at 21:33 UT (420 s after launch) (courtesy G.Webb). The *white dot* indicates the location of the payload projected along the magnetic field direction down to 110 km at that time. The *black dots* show the locations at 21:30 (240 s) and 21:31 UT (300 s), respectively. The *star in the upper left-hand area* is Alkaid

Observations

The observations pertaining to small-scale field-aligned current flow were made during the time interval 190–260 s after launch. As can be seen from Figs. 2 and 3, the payload was near the northern boundary of the auroral activity at this time. Visual and television observations in Fig. 7 show more clearly than Fig. 3 that the region in question was occupied by discrete auroral arcs with a pronounced ray structure. This is supported by the measurements of low-energy electron fluxes given in Fig. 8. As long as the instrument was in the appropriate mode, highly-structured, intense electron precipitation was detected followed by steep decreases in numbers as well as energy fluxes, shortly after 260 s elapsed time. North of this region the energy flux carried by low-energy electrons in the range 0.1–25 keV was smaller than 10^{-2} erg cm^{-2} s^{-1}, whereas inside the area with auroral activity the energy flux was nearly three orders of magnitude higher. A conspicuous spike between 210 and 220 s elapsed time is investigated in detail in Fig. 9. The lower curves of this figure and of Fig. 10 are the magnetic field variations derived from the fluxgate magnetometer measurements. The originally spin- and coning-modulated magnetometer data have been transformed into an earth-fixed coordinate system. B_x points towards magnetic north, B_y towards magnetic east, and B_z downwards parallel to the undisturbed geomagnetic field. A reference field was deduced from the transformed measurements to obtain the variations of the magnetic field vector. The data shown cover the times 190–226 s and 230–260 s after launch, respectively. Activation of the attitude control system affected the magnetic field measurement during the missing time section. No magnetic field variations were observed in B_z. B_x shows some variations at frequencies of a few Hz between 210 and 216 s. Short-period variations were observed in the same time interval in B_y. In addition, B_y increased between 190 and 211 s. A decrease in B_y is seen from 211 to 216 s. The short-period variations can be explained in terms of hydromagnetic waves (Klöcker and Theile 1979). The event in Fig. 10, occurring half a minute later, showed very similar signatures. The low-energy electron experiment had switched to another mode allowing high-time-resolution measurements at the expense of spectral information. The low-energy electron flux decreased by two orders of

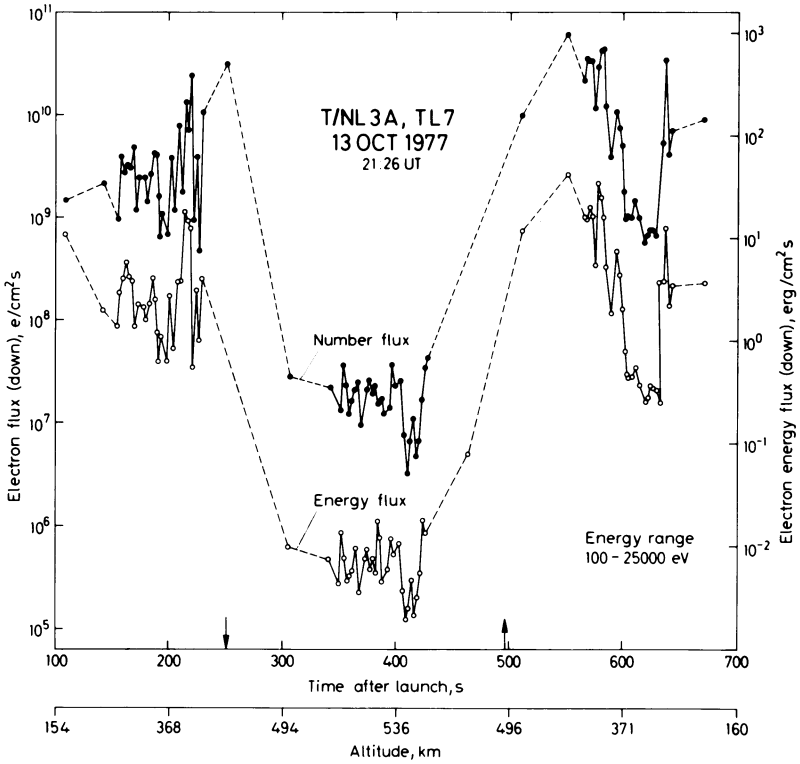

Fig. 8. Summary diagrams of the electron number flux and energy flux during flight 3A. The different time resolution apparent in this figure results from different operating modes of the instrument

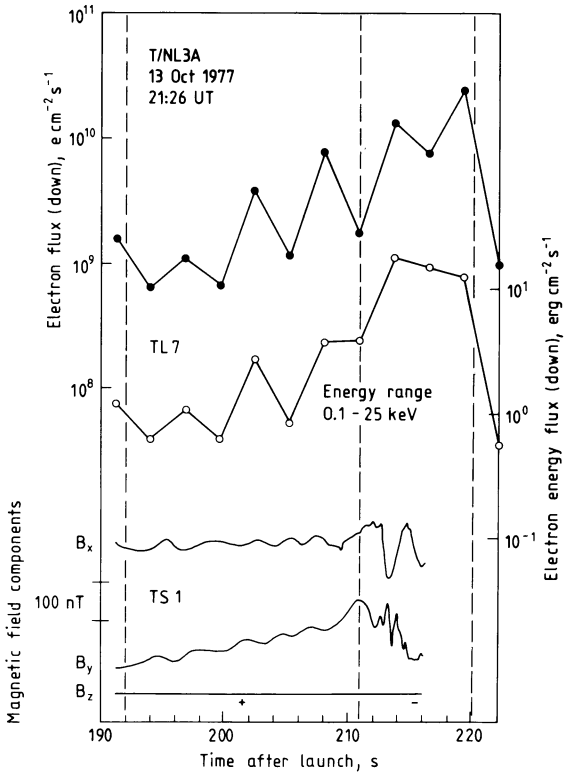

Fig. 9. Comparison between electron flux data and magnetic field observations made aboard payload T/NL 3A during the time interval 192–220 s elapsed time. The apparent, smooth wave forms occurring coherently in the B_x and B_y components result from residual spin contributions to the magnetic field variations measured aboard the moving payload. Regions marked + and − are characterized by downward- and upward-directed currents, respectively

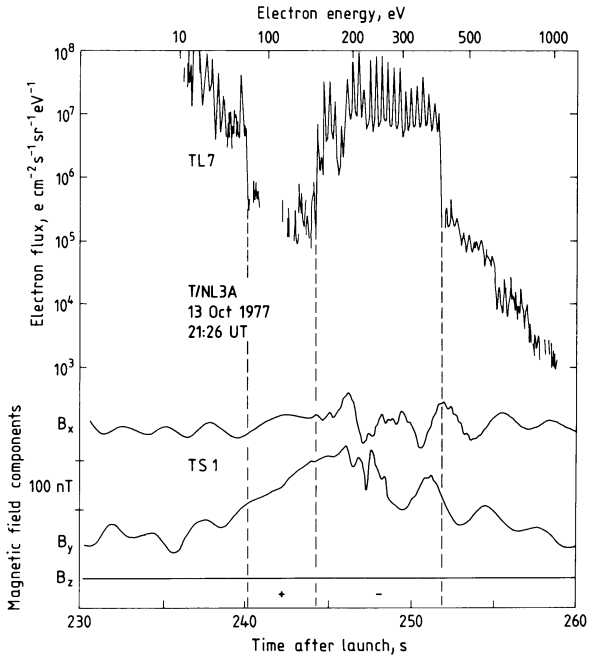

Fig. 10. High time-resolution electron flux measurements as compared to magnetic field observations made aboard payload 3A between 230 and 260 s elapsed time. The magnetic field observations have been given in the same format as in Fig. 9. The electron data were obtained in a slow energy scan mode with an energy increment every spin period. The spin modulation present near 250 s resulted from a field-aligned electron flux distribution. The lack of detailed correspondence between particle and field data is not surprising in view of the fact that the magnetometer observations represent an integrated response to an extended current distribution

magnitude between 240.1 and 243.9 s and after 251.6 s elapsed time. It is important to note that all three variations occurred within one spin period each, while the experiment was set on fixed energy levels. Consequently, they have to be considered as time-space variations rather than spectral features. The apparent modulation of the electron flux resulted from a pitch angle anisotropy with fluxes peaked along the magnetic field direction. A model pitch angle distribution of $F(\alpha) \sim 40 \cos^{12}\alpha + 1$ for $0 \leqq \alpha \leqq 90$ and $F(\alpha) \sim 1$ for $90 \leqq \alpha \leqq 120$ best fits the data in the energy range 200–370 eV.

In both cases, the magnetic data suggest that the payload encountered field-aligned electric current sheets with downward-directed currents at the southern boundary and upward-directed currents north of it. The low-energy electron flux observations support this interpretation as far as the upward-directed current is concerned by identifying intense electron fluxes flowing along the magnetic field lines into the ionosphere. On the other hand, very low fluxes were measured in the regions of downward currents.

These interesting events seem to merit extensive investigation making full use of the available data set provided by this payload. Energy spectra of the low-energy electrons were measured with high time-resolution during the first event and have been displayed in Fig. 11. Before and after the event the spectrum can be approximated by a single power law function $F(W) \sim W^{-\gamma}$, with exponent $\gamma = 2.3$. During the period with increased flux the spectrum changed considerably. This spectral variation was accompanied by a change in the directional distribution. In the energy range 0.1–0.6 keV, the pitch angle distribution peaked along the magnetic field direction with a best-fit model of approximately $F(\alpha) \sim 50 \cos^{15}\alpha + 1$ for angles of $0 \leqq \alpha \leqq 90$. At higher energies, near 2 keV, the distribution was also field-aligned as can be seen from Fig. 12 where, in addition, a model fit of $F(\alpha) \sim 10 \cos^{15}\alpha + 1$ is shown.

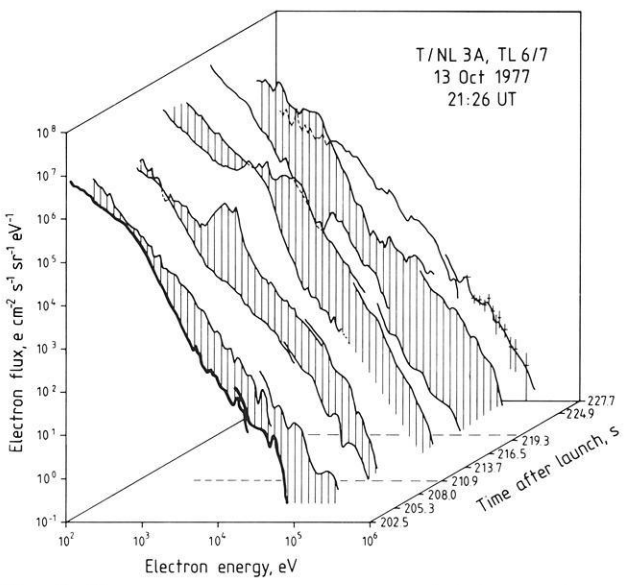

Fig. 11. Electron energy spectra as measured during the first of the events described. The observations were made by two instruments in different energy ranges with some overlap near 25 keV. A spectral peak developed between 210.9 and 216.5 s near 2 keV accompanied by an increase of the flux near 25 keV of more than an order of magnitude. Representative statistical errors have been indicated. At lower energies statistical errors are insignificant. The intervals of the first upward-directed current sheet has been marked by *broken lines*

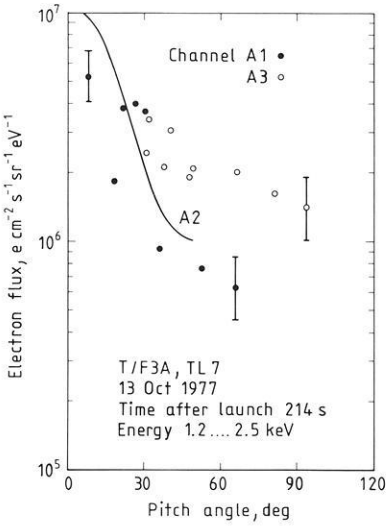

Fig. 12. Pitch angle distribution of 1.2–2.5 keV electrons at 214 s after launch measured by three different instrumental channels. Channels A1 and A3 provided directional observations. The field-aligned electron flux described by the model function $10 \cos^{15}\alpha + 1$ (*solid line*) was deduced from channel A2, with fan-shaped viewing cone covering 96°. Statistical errors are small. The absolute errors for the directional channels have been estimated to be approximately $\pm 20\%$ while channel A2 should be accurate to $\pm 10\%$

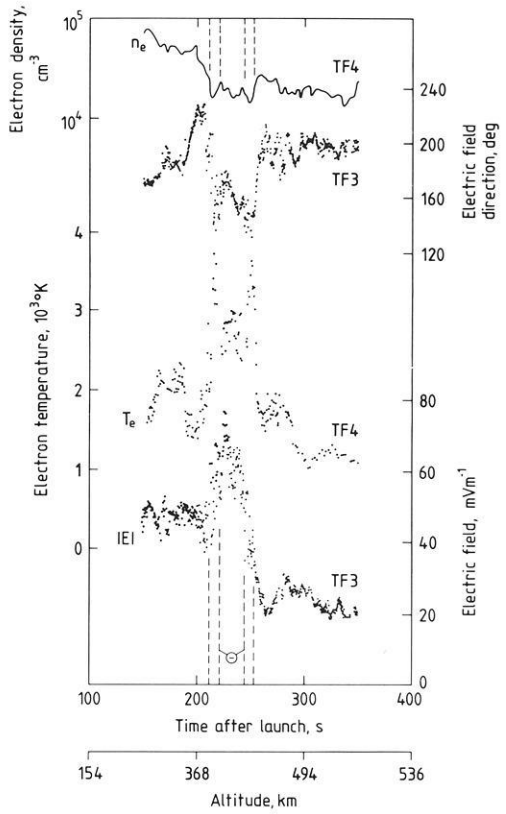

Fig. 13. Electron density, electric field direction, electron temperature and electric field intensity as functions of time after launch and altitude. The regions of upward-directed field-aligned currents have been marked by – and *broken lines*

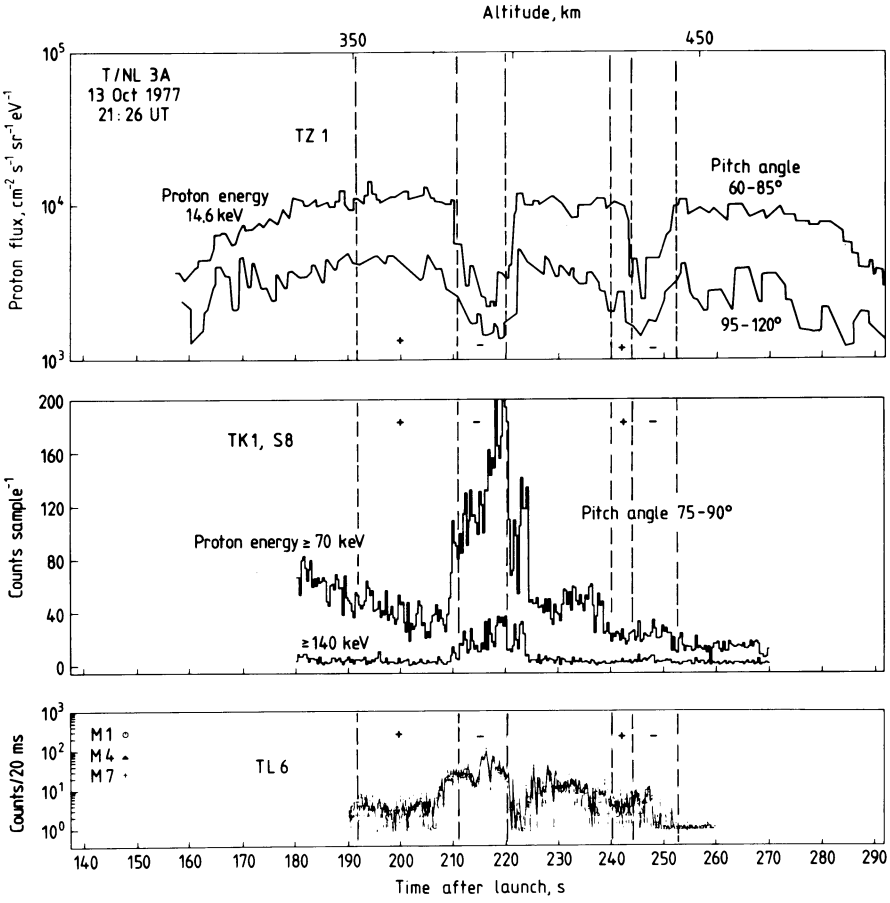

Fig. 14. Energetic proton and electron observations. Both current sheets affected the 14.6 keV proton flux significantly as shown in the *upper graphs*. The high-energy proton flux as well as the electron flux (*middle and lower part*) increased during the first current sheet encounter, but showed no significant effect during the second. Three electron channels $E >$ 15 keV have been plotted (M1: pitch angle $\approx$ 20°, M4: 5°–45° and M7: 30°–70°). The high energy proton data cover the pitch angle domain 75°–90° and were taken when the viewing cone was looking in westward directions. Regions of upward- and downward-directed current flow have been indicated

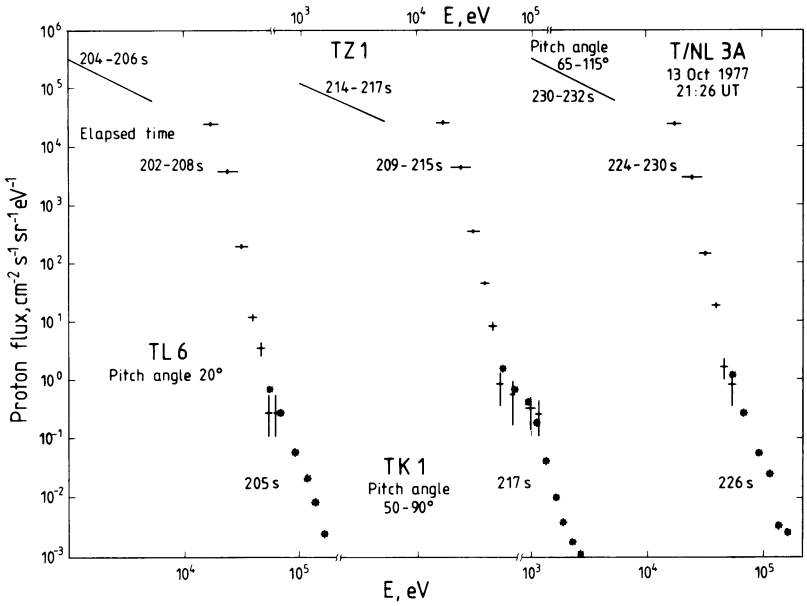

Fig. 15. Proton spectra observed before, during and after the first current sheet crossing by three different instruments. The low-energy depression and the high energy enhancement shown in Fig. 14 can be understood as spectral changes of the proton population

Physical effects related to the current sheets as seen by the low-energy electron and magnetometer experiments were also observed by the other instruments. First, we present plasma data from the retarding potential analyser and electric field experiments in Fig. 13. The density of the thermal electrons dropped by a factor of roughly two during the time intervals with upward-directed currents, whereas the electron temperatures increased from values near 1,500° to 3,500° K attaining their peak values exactly inside the regions with upward-directed currents. The data presented in Fig. 13 suggest, however, that both current sheets did not occur independently, but were generated by a common process. The electric field measurements presented in the lower portions of this figure show abrupt variations both in intensity and in direction. Specifically, the quasistatic electric field increased

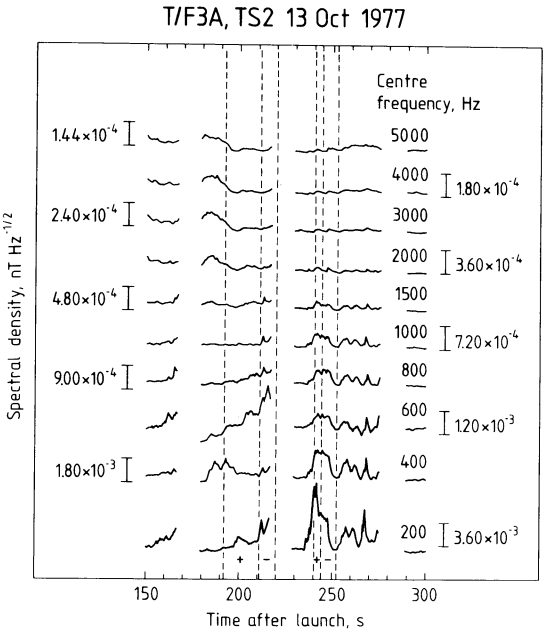

Fig. 16. Magnetic wave field observations in several frequency bands each having 100 Hz band width. The instrument suffered from interference when the attitude control system was activated and the data could not therefore be evaluated continuously. Enhancements of the magnetic fluctuations in the lower frequency bands seem to be related to the currents sheets, although a one-to-one correspondence can not be seen

from 40 to 80 mV/m during the first interval and decreased from approximately 60 to 20 mV/m in the course of the second event while the azimuth of the electric field direction varied between about 200 and 110° in both cases.

A summary of the energetic proton and electron observations has been compiled in Fig. 14. The important point to note is that the low-energy channel at 14.6 keV is clearly anticorrelated with the electron flux whereas the high-energy proton flux shows a positive correlation with the electrons during the periods of upward-directed electric currents. The proton spectra given in Fig. 15, for a time interval covering the first current-sheet encounter, demonstrate that the proton flux near 30 keV had been relatively constant. At energies below this level flux decreases were observed, whereas enhancements were present at higher energies. In particular, the high energy tail above 60 keV should be mentioned, as well as the fact that the high-energy proton flux was field-aligned in the electron precipitation region.

The observations of the perpendicular magnetic wave field given in Fig. 16 show increased activity in all frequency bands from 200–2,000 Hz in relation to the current layers, however, a clear one-to-one correspondence could not be detected. The spectral densities at different centre frequencies are given with a bandwidth of 100 Hz. The pulses of the attitude control system have been suppressed in this figure. There is some enhancement at 400 Hz between 185 and 200 s. A more pronounced noise level can be seen between 240 and 270 s. The maximum amplitude is at 200 Hz or below. This observation is consistent with results of Gurnett and Frank (1972), who found that inverted "V" events and ELF-noise very often occurred simultaneously. No satisfying physical explanation is yet available. Spectrograms of the AC electric field covering the whole of this flight exhibit a strong hiss signal with a cut off at the lower hybrid frequency near 7 kHz without any pronounced structures related to the current sheet encounters.

Discussion

The all-sky camera data, the low-energy electron fluxes, the electron temperature and the electric field characteristics all suggest that the payload reached the northern boundary of the auroral oval shortly after 251 s elapsed time. Whether the observed structures were of spatial or temporal type could not be determined unambiguously from the rocket data alone. Since the auroral activity regions and the large-scale electrojet were, however, stationary in latitude during this time interval, it can be concluded that the payload traversed spatial structures with a velocity of approximately 1,100 ms^{-1} normal to the magnetic field lines. The abrupt transitions from one plasma regime to the other, apparent in the electron data of Fig. 10, occurred over a distance of about 70 m. It also follows that the double sheet near 250 s had a total thickness of 13 km, of which 8 km were occupied by the upward-directed current. The corresponding figures as determined from the magnetometer measurements were 12 and 7 km, respectively. The width of the upward-directed current sheet centred near 215 s was 10 km and it was separated from the sheet at 250 s by approximately 38 km. Structures with a width of only several 100 m as quoted by Kan et al. (1979) could not be found although the resolution of the instruments would have been sufficient for an unambiguous detection. In addition to the good agreement as far as the width of the current sheets is concerned, the evaluation of the current densities in the upward-directed current regions led to reasonable agreement between the field and particle data. Assuming a current sheet of infinite extent and a payload motion perpendicular to it, the current density can be related to the magnetic field according to $j=(1/\mu_0)dB/dx$. The downward current cannot be determined from the electron precipitation data. The relevant parameters of the current sheets as far as they could be determined from the observations have been compiled in Table 2.

The current density values as derived from the electron flux data should, however, be qualified in two respects. Firstly, it should be noted that the upward-directed electron flux was only measured in the pitch angle range 90–120° and, secondly, observations were not available over the full energy range. The fact that in both cases the electron data yield higher current densities might indicate an under-estimation of the return flux of energetic electrons contained implicitly in the model pitch angle distributions. The current densities were several times larger than the threshold density of 2.5 μAm^{-2} for auroral arc spiral formation (Davis and Hallinan 1976; Hallinan 1976).

The plasma measurements demonstrate that the two different current regimes were populated by different electron distributions. A low-density, high-temperature electron gas was observed in the upward-directed current sheet and a high-density, low-temperature one in the adjacent region. As the events were observed by this payload at an altitude of approximately 400 km, the conclusion can be drawn that magnetospheric electron populations were carried down to at least that altidue. The strong field alignment of the energetic electron fluxes confirms the concept that low-altitude electric fields parallel to the magnetic lines of force exist above the auroral ionosphere. Judging from the positions of the peak and knee in the spectral electron distributions in Fig. 11, the maximum potential drop during the 210 s event was approximately 4 kV. The data discussed so far consistently describe current sheets connecting the outer magnetosphere with the ionosphere during the main phase of a magnetospheric substorm. We will now attempt to relate the additional information to these structures.

Table 2. Current sheet parameters

Event	192–211 s	211–220 s	240–244 s	244–252 s
Current direction	Downwards	Upwards	Downwards	Upwards
Width, km				
Magnetic data[a]	9	–	8	7
Electron data[b]	–	10	5	8
Current density, μAm^{-2}				
Magnetic data	13	25	18	17
Electron data	–	40	–	22

[a] Width deduced depends on details of current sheet structure in E-W direction. Values given refer to simple E-W extending sheets. Spirals as indicated in Fig. 3 would tend to broaden the width

[b] Width calculated assuming perpendicular traverses

The electric field measurements exhibit large variations in amplitude as well as in azimuth across the current sheet structures. It has already been noted that the electric field data clearly relate the observed current sheets to a single feature characterized by an increase in the electric field intensity and a distinct change in the direction. In an attempt to identify this structure, the electric field information provided by the STARE system (Greenwald et al. 1978) was compared with the sounding rocket data and the auroral observations in Fig. 17. A study by Cahill et al. (1978) showed good agreement between electric fields determined from STARE and sounding rocket data. The bright auroral arc denoted by *A* delineated a change in the direction of the electric field in all three intervals. In region *B* between the bright arc *A* and the northern edge of the auroral activity, southward directed fields prevailed. Neither an intensification nor a variation of the direction could be detected near the arc *C* at 71–72° latitude, as would have been expected from the rocket measurements during the current sheet encounters. Besides this difference, there was a general disagreement between the electric field magnitude observed by the rocket instrument and STARE. The radar beam covering the trajectory of the payload was however not operating satisfactorily thus precluding any detailed comparison. Nevertheless, it can be inferred from Fig. 17 that the current sheets were encountered at the northern boundary of a region with electric fields above the STARE threshold having a latitudinal extension of several hundred kilometres and a southward direction.

The electron flux observations have provided evidence that the field-aligned current sheets were accompanied by quasi-static electric potential differences along the magnetic field lines. Such a configuration, if directed so as to accelerate electrons downwards, should of course decelerate precipitating protons and indications of such an effect could indeed be found at the low-energy end of the observations presented in Figs. 14 and 15. The enhancement of both the energetic electron and proton fluxes accompanying the current sheet at 210–220 s point to another process related to the various phenomena. This is particularly true for the high-energy tail of the proton spectrum at 209–215 s.

The energetic particle fluxes during the second current-sheet encounter were considerably lower, in line with a general decrease of the mean energy of the low-energy electron population from approximately 6 keV near the bright auroral arc to 0.1 keV at the northern edge of the auroral activity, which can be determined using the data shown in Fig. 8.

In summary, the observations presented here demonstrate that field-aligned current sheets having current densities in excess of 10 μAm^{-2}, with opposite directions, occurred near the northern

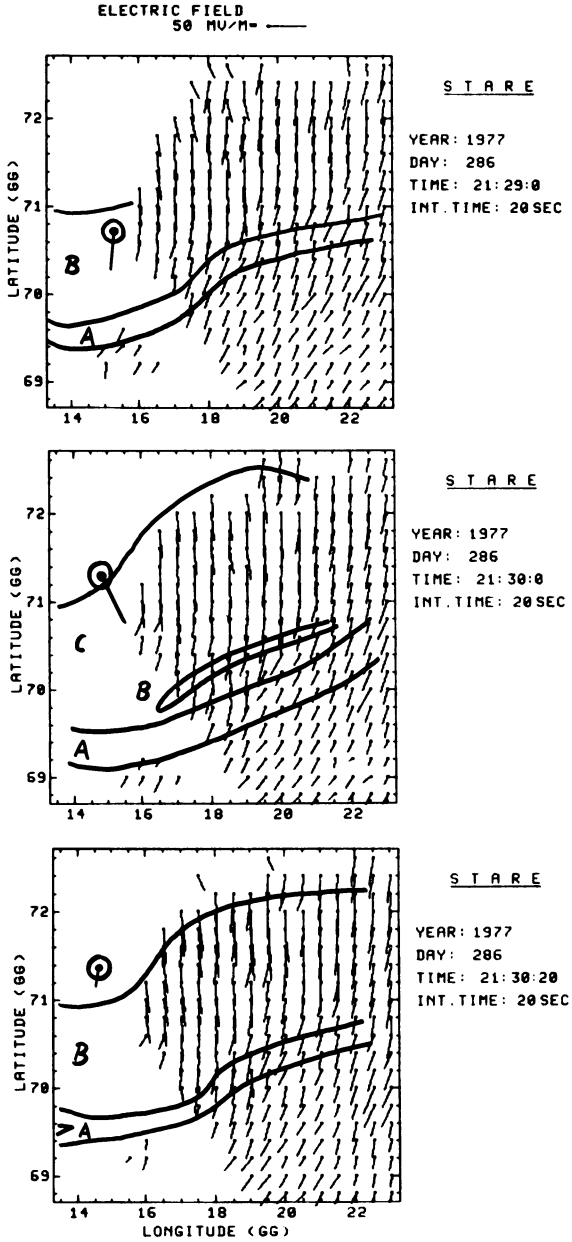

Fig. 17. Ionospheric electric fields as derived from STARE observations for three integration intervals during the first part of the sounding rocket flight 3A. Also shown are the positions of the bright auroral arcs (*lines*) as well as the electric field observed aboard the rocket and projected down to 100 km along the magnetic field direction (*circles*). The observations were made at 180, 240, and 260 s after launch with an integration time of 20 s

edge of an auroral break-up region. The sheets could be related to active discrete auroral forms. The sheet parameters, current density and latitudinal width, as determined by the on-board magnetometer and electron spectrometer instruments, were in reasonable agreement. In particular, it could be concluded that the upward current was carried predominantly by energetic electrons. The widths of the sheets ranged from 5–10 km. Although the instrumentation was capable of resolving narrower structures, such features were not observed. The edges of the different plasma regimes were extremely sharp accompanied by quasi-static electric field transitions as well as magnetic ULF and VLF wave field

activity. The plasma parameters could be characterized by decreases in the electron density and strong enhancements of the electron temperature. High-energy charged particle measurements indicated that very energetic processes were involved in the generation mechanisms of these structures, while low-energy electron and proton observations provided strong evidence of field-aligned acceleration and deceleration within the upward-directed current sheets. The lack of any detailed correspondence between both the magnetic and electric AC fields and the other current sheet parameters points to a propagation effect and thus to the fact that the interaction region was located away from (presumably above) the observation point.

Acknowledgements. Many individuals at the various institutions contributed to this sounding rocket programme. In particular, we should like to mention Dr. Hörle as project manager of DFVLR-PT. We also want to thank the integration team of Dornier System, the DFVLR launch team and the personnel of the Andøya Rocket Range for their support of the project. The work was supported financially by the German Bundesministerium für Forschung und Technologie and by the Austrian Akademie der Wissenschaften. Drs. R.A. Greenwald and E. Nielsen kindly provided the STARE data used in this study.

References

Anderson, H.R., Vondrak, R.R.: Observations of Birkeland currents at auroral latitudes. Rev. Geophys. Space Phys. **13**, 243–262, 1975

Armstrong, J.C., Akasofu, S.-I., Rostoker, G.: A comparison of satellite observations of Birkeland currents with ground observations of visible aurora and ionospheric currents. J. Geophys. Res. **80**, 575–586, 1975

Baumjohann, W.: Spatially inhomogeneous current configurations as seen by the Scandinavian Magnetometer Array. In: Proceedings of the International Workshop on Selected Topics of Magnetospheric Physics, Japanese IMS Committee, ed.: pp. 35–40. Tokyo 1979

Baumjohann, W., Sulzbacher, H., Potemra, T.A.: Joint magnetic observations of small-scale structures in a westward electrojet with Triad and the Scandinavian Magnetometer Array. In: Procedings of the International Workshop on Selected Topics of Magnetospheric Physics, Japanese IMS Committee, ed.: pp. 49–52. Tokyo 1979

Bryant, D.A., Hall, D.S., Lepine, D.R., Mason, R.W.N.: Electrons and positive ions in an auroral arc. Nature **266**, 148–149, 1977

Cahill, L.J., Jr., Greenwald, R.A., Nielsen, E.: Auroral radar and rocket double-probe observations of the electric field across the harang discontinuity. Geophys. Res. Lett. **5**, 687–690, 1978

Cattell, C., Lysak, R., Torbert, R.B., Mozer, F.S.: Observations of differences between regions of current flowing into and out of the ionosphere. Geophys. Res. Lett. **6**, 621–624, 1979

Croley, D.R., Mizera, P.F., Fennell, J.F.: Signature of a parallel electric field in ion and electron distribution in velocity space. J. Geophys. Res. **83**, 2701–2705, 1978

Davis, T.N. and Hallinan, T.J.: Auroral spirals. 1. Observations. J. Geophys. Res. **81**, 3953–3958, 1976

Evans, D.S.: Precipitating electron fluxes formed by a magnetic field aligned potential difference. J. Geophys. Res. **79**, 2853–2858, 1974

Greenwald, R.A., Weiss, W., Nielsen, E., Thomson, N.R.: STARE: A new radar auroral backscatter experiment in northern Scandinavia. Radio Sci. **13**, 1021–1039, 1978

Gurnett, D.A., Frank, L.A.: ELF noise bands associated with auroral electron precipitation. J. Geophys. Res. **77**, 3411–3417, 1972

Gustafsson, G.: A revised corrected geomagnetic coordinate system. Ark. Geofys. **5**, 595–617, 1970

Hallinan, T.J.: Auroral spirals, 2. Theory. J. Geophys. Res. **81**, 3959–3965, 1976

Hughes, T.J., Rostoker, G.: Current flow in the magntosphere and ionosphere during periods of moderate activity. J. Geophys. Res. **82**, 2271–2282, 1977

Hughes, T.J., Rostoker, G.: A comprehensive model current system for high-latitude magnetic activity – I. The steady state system. Geophys. J. R. Astron. Soc. **58**, 525–569, 1979

Kan, J.R., Akasofu, S.-I.: A model of the auroral electric field. J. Geophys. Res. **84**, 507–512, 1979

Kan, J.R., Lee, L.C., Akasofu, S.-I.: Two-dimensional potential double layers and discrete auroras. J. Geophys. Res. **84**, 4305–4315, 1979

Kaufmann, R.L., Walker, D.N., Arnoldy, R.L.: Acceleration of auroral electrons in parallel electric fields. J. Geophys. Res. **81**, 1673–1682, 1976

Klöcker, N., Theile, B.: Magnetic ULF-waves in the vicinity of active auroral forms. J. Geophys. **46**, 229–236, 1979

Küppers, F., Untiedt, J., Baumjohann, W., Lange, K., Jones, A.G.: A two-dimensional magnetometer array for ground-based observations of auroral zone electric currents during the International Magnetospheric Study (IMS). J. Geophys. **46**, 429–450, 1979

Mende, S.B., Shelley, E.G.: Coordinated ATS 5 electron flux and simultaneous auroral observations. J. Geophys. Res. **81**, 97–110, 1976

Mersmann, U., Baumjohann, W., Küppers, F., Lange, K.: Analysis of an eastward electrojet by means of upward continuation of ground-based magnetometer data. J. Geophys. **45**, 281–298, 1979

Mizera, P.F., Fennell, J.F.: Signatures of electric fields from high and low altidue particles distribution. Geophys. Res. Lett. **4**, 311–314, 1977

Pellinen, R.J., Heikkila, W.J.: Observations of auroral fading before breakup. J. Geophys. Res. **83**, 4207–4217, 1978

Raitt, W.J., Sojka, J.J.: Field-aligned suprathermal electron fluxes below 270 km in the auroral zone. Planet. Space Sci. **25**, 5–13, 1977

Sharp, R.D., Johnson, R.G., Shelley, E.G.: Energetic particle measurements from within ionospheric structures responsible for auroral acceleration processes. J. Geophys. Res. **84**, 480–488, 1979

Swift, D.W.: Mechanisms for the discrete aurora – a review. Space Sci. Rev. **22**, 35–75, 1978

Swift, D.W.: On the structure of auroral arcs: The results of numerical simulations. J. Geophys. Res. **84**, 469–479, 1979

Theile, B., Praetorius, H.M.: Field-aligned currents between 400 and 3000 km in auroral and polar latitudes, Planet. Space Sci. **21**, 179–187, 1973

Whalen, B.A., Daly, P.W.: Do field-aligned auroral particle distributions imply acceleration by quasi-static parallel electric fields? J. Geophys. Res. **84**, 4175–4182, 1979

Wilhelm, K.: Auroral particle fluxes in the ionosphere. J. Geophys. **46**, 151–169, 1979

Wilhelm, K.: Study of magnetospheric substorm events. Proceedings of the Vth ESA Symp. on European Rocket and Balloon Programmes and Related Research. ESA Special Publication **152**, 269–277, 1980

Zmuda, A.J., Armstrong, J.C., Heuring, F.T.: Characteristics of transverse magnetic disturbances observed at 1,100 km in the auroral oval. J. Geophys. Res. **75**, 4757–4762, 1970

Received July 1, 1980; Revised Version November 14, 1980
Accepted December 22, 1980